Nanoscale

Accepted Manuscript

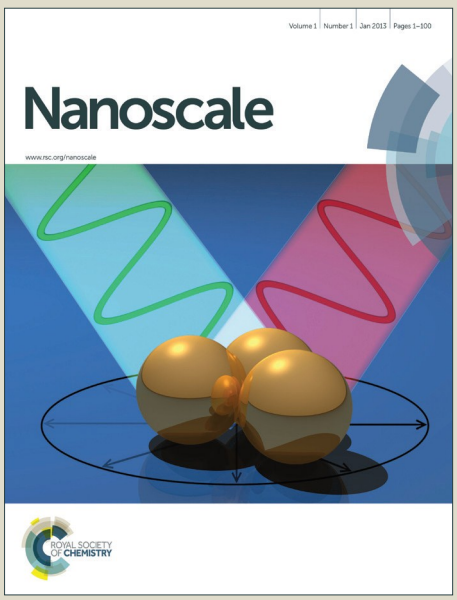

ROYAL SOCIETY OF CHEMISTRY

www.rsc.org/nanoscale

Cite this: DOI: 10.1039/c0xx00000x

www.rsc.org/xxxxxx

ARTICLE TYPE

Preparation of fluorescent mesoporous hollow silica-fullerene nanoparticle via selective etching for combined chemotherapy and photodynamic therapy

Yannan Yang,[a] Meihua Yu,*[a] Hao Song,[a] Yue Wang[a] and Chengzhong Yu*[a]

Received (in XXX, XXX) Xth XXXXXXXXX 20XX, Accepted Xth XXXXXXXXX 20XX
DOI: 10.1039/b000000x

Well-dispersed mesoporous hollow silica-fullerene nanoparticles with particle sizes of ~ 50 nm have been successfully prepared via incorporating fullerene molecules into silica framework followed by a selective etching method. The fabricated fluorescent silica-fullerene composite with high porosity demonstrates its excellent performance in combined chemo/photodynamic therapy.

Mesoporous silica nanoparticles (MSNs) are promising nanocarriers for cancer therapy due to their tunable chemical and physical properties and excellent biocompatibility.[1] Among various types of silica based materials, MSNs with a hollow structure are of great interest due to the presence of inner cavity, which allows an enhanced drug storage capacity.[2] The preparation of hollow nanostructures is mostly dependent on hard templating[3] and soft templating[4] methods, which generally use toxic organic solvent or surfactant for synthesis and harsh conditions for template removal. The selective etching strategy to prepare hollow silica nanoparticles was firstly reported by Shi and coworkers.[5] Afterwards, remarkable progress in understanding the inhomogeneity of silica framework formed by Stöber method has led to development of a facile selective etching strategy to directly convert solid structure into hollow structure.[6,7] This interesting finding inspired us to consider the possibility of extending this strategy into other silica synthetic systems, in order to prepare silica based porous materials with advanced biomedical functions and performance.

Cancer therapy relying on a single therapeutic strategy generally suffers from unsatisfactory efficiency as well as severe side effects.[8] Combination of multiple therapeutic methodologies with different mechanisms has been considered as a promising alternative to overcome these drawbacks.[9] For instance, photodynamic therapy (PDT), as a recently developed alternative method to traditional cancer treatments, has been combined with chemotherapy to achieve enhanced therapeutic efficiency with lower drug dosages.[10] PDT is based on the concept that the photosensitizer (PS) is activated by a specific wavelength of light and results in generation of singlet oxygen ($^1O_2$) in the presence of molecular oxygen to induce cancer cell death.[11] Fullerene (C_{60}), which possesses mild fluorescence under exposure of visible light and the highest efficiency of $^1O_2$ formation among all the PS molecules investigated so far,[12] has attracted considerable interest in biomedical applications. To date, most reports on the C_{60} based PDT rely on conjugation of hydrophilic polymers to enhance the dispersity of C_{60} nanoparticles in physiological condition.[10a, 10b, 10d] However, aggregation of C_{60} molecules is inevitable in those systems, which results in $^1O_2$ quenching and extremely low fluorescent intensity.[13] Jeong et al. have demonstrated the great potential of C_{60} incorporated silica nanoparticles in bio-imaging application owing to their high photoluminescence and remarkable photostability.[14] However, those nanostructures are lack of porosity, which is believed fairly disadvantageous for the interaction between C_{60} and molecular oxygen[11] as well as additional drug loading. Taking the advantage of intrinsic hydrophilic property and tunable porous structure of silica, we expect that porous silica nanoparticles with incorporated C_{60} can be developed as a novel multifunctional cancer therapeutic platform with several advantages: enhanced photodynamic activity, sufficient drug loading capacity, well-preserved fluorescence, good water dispersity and excellent biocompatibility.

Herein, we report a facile preparation of mesoporous hollow silica-fullerene (MHSF) nanoparticles using a selective etching method. Our designed MHSF is a three-in-one system: The inner cavity serves as a reservoir to encapsulate drugs for chemotherapy, while the C_{60} molecules incorporated in silica shell act as PS for PDT as well as fluorescent agent for imaging. The porous silica shell not only ensures the accessibility of the inner cavity, but also enhances the PDT efficiency by facilitating the interaction between C_{60} and molecular oxygen and the release of $^1O_2$. To our knowledge, this is the first report on mesoporous silica-C_{60} based multifunctional system for simultaneous chemo-/photodynamic therapy and fluorescent imaging.

The preparation route of MHSF is depicted in Scheme 1. A solid silica-fullerene nanoparticle (SSF) was first prepared using reverse microemulsion method as starting materials[14] (Scheme 1A), which was further subjected to ethanol-thermal treatment before etching in diluted ammonia solution to obtain a hollow structure with mesoporous silica shell (Scheme 1B, see details in experimental section, supporting information). The obtained MHSF is further loaded with doxorubicin for chemotherapy, while the C_{60} molecules incorporated in the mesoporous silica shell are able to generate $^1O_2$ and fluorescence under light excitation for PDT and imaging, respectively (Scheme 1C).

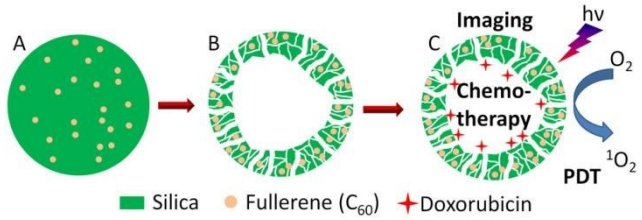

Scheme 1 Schematic illustration of the preparation procedure of MHSF for applications in imaging and combined chemo-/photodynamic therapy.

Transmission electron microscope (TEM) images of SSF and MHSF are shown in Figure 1. Uniform and well dispersed nanoparticles with particle sizes of 50±7 nm (by counting 50 nanoparticles) can be observed for both SSF and MHSF (Figures 1a, b). SSF shows a solid structure, while after selective etching treatment, more than 90% of MHSF shows a hollow structure. At a higher magnification, the entrance on the shell of MHSF can be clearly observed (indicated by black arrows), which is estimated of ~ 10 nm (Figure 1c). The hollow structure and entrance on the silica shell is further evidenced by electron tomography (ET) technique (Figure 1d). Figure 1c inset reveals that MHSF can be well dispersed in aqueous solution with yellow colour, which is attributed to the incorporated C_{60} molecules. The dynamic light scattering (DLS) measurement reveals that both SSF and MHSF have a hydrodynamic diameter of 61 nm (Figure S1), which is slightly larger than that measured from TEM due to the surface hydration.[15] The small polydispersity index (PDI) values in both particles suggest their uniform particle sizes and excellent aqueous dispersity.

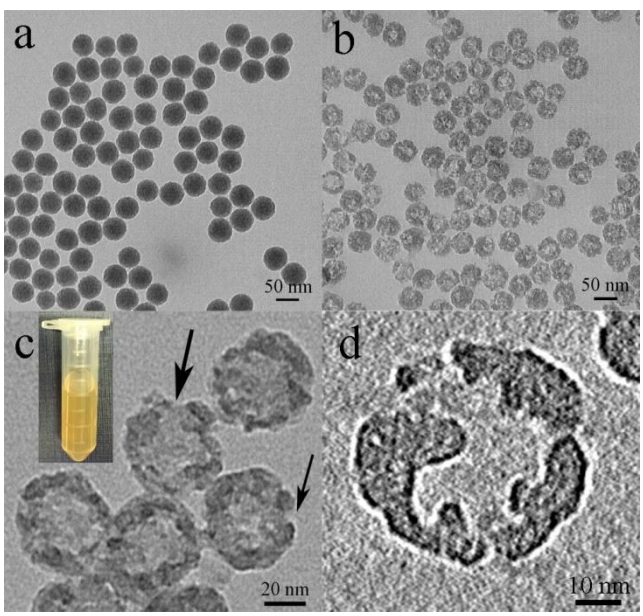

Fig.1 TEM images of SSF (a), MHSF (b, c) and one ET slice of MHSF (d). Black arrows indicate the entrance on the silica shell. Inset is a digital image of MHSF suspension in water.

To further confirm the presence of C_{60} molecules in MHSF, the chemical composition of the MHSF and pure silica are compared and analyzed with several characterization techniques. The pure silica was prepared as a control following exactly the same procedure of SSF but without adding C_{60}. Fourier transform infrared spectroscopy (FTIR) spectra of MHSF and pure silica are shown in Figure S2. The aromatic C=C stretching peak (1509 cm^{-1}) is observed exclusively in the MHSF spectrum, indicating the presence of C_{60}. The UV-Vis absorption spectrum of MHSF (Figure S3) exhibits three very weak peaks at 223, 267 and 358 nm, which is attributed to the incorporated C_{60} with absorbance at 210, 254, and 326 nm.[14] The shift of peak position can be explained by the altered electronic energy levels of C_{60} that forms chemical bond with silica framework.[14] To quantitatively measure the C_{60} content, elemental analysis was conducted for both SSF and MHSF. Pure silica contains 2.5 ± 0.2% carbon, which is mainly due to the incompletely hydrolyzed tetraethyl orthosilicate (TEOS) and organic residues. SSF and MHSF contain more carbon than pure silica (7.8 ± 0.3% and 7.5 ± 0.2%, respectively), which is contributed by the incorporated C_{60}. This similar content of C_{60} before and after selective etching indicates the homogeneous distribution of C_{60} molecules in silica frameworks.

The nitrogen adsorption-desorption plots of SSF and MHSF show both type IV isotherm according to the IUPAC nomenclature (Figure S4). The desorption branch of MHSF exhibits a steep capillary evaporation step at P/P_0 ~ 0.8, indicating a large entrance size. For sample SSF, the capillary evaporation step occurs at P/P_0 ~ 0.9, which is attributed to the N_2 desorbed from inter-particle packing voids. The corresponding entrance size of MHSF is calculated to be 11.2 nm (Figure S4 inset), consistent with TEM observation. The Brunauer–Emmett–Teller (BET) surface area of sample SSF and MHSF is 45.6 and 331.9, m^2 g^{-1}, respectively, while the total pore volume is 0.36 and 1.1 cm^3 g^{-1}, respectively (Table S1). The greatly increased surface area and pore volume of MHSF compared to that of SSF suggest significantly higher porosity, which is important for the following enhanced PDT performance and drug loading capacity.

To compare the generation efficiency of $^1O_2$ produced by SSF and MHSF, 9,10-anthracenediyl-bis(methylene) dimalonic acid (ABDA) was used as a $^1O_2$ sensor.[10b] After chemical reaction with $^1O_2$, ABDA is bleached to endoperoxide, which results in a decrease in optical density (OD) at 376 nm (λ_{max} of ABDA).[10b] Figure 2 shows the OD changes in different sample dispersions in pure deuterium oxide (D_2O) as a function of UV light exposure time. In the presence of SSF, the OD at 376 nm gradually decreased as the exposure time increases (Figure 2a). Such a decreasing trend is more significant in the presence of the same concentration of MHSF (Figure 2b), suggesting that MHSF is capable of generating increased amount of $^1O_2$. MHSF with enhanced porosity in the silica framework (Table S1) allows an improved availability of molecular oxygen molecules to interact with C_{60}, thus more $^1O_2$ can be generated in MHSF. In contrast, ABDA solution shows a negligible decrease in OD with time (Figure 2c), confirming that the bleaching of ABDA is not caused by the UV light irradiation. Results from Figure 2a-c are also plotted in Figure 2d for comparison, revealing that the bleaching of ABDA is time-dependent under UV irradiation in the presence of C_{60} incorporated nanoparticles, while the normalized OD value of ABDA with MHSF is almost half compared to that of ABDA with SSF. Thus, it is suggested that MHSF can act as a more powerful photodynamic therapeutic agent.

Cite this: DOI: 10.1039/c0xx00000x
www.rsc.org/xxxxxx

ARTICLE TYPE

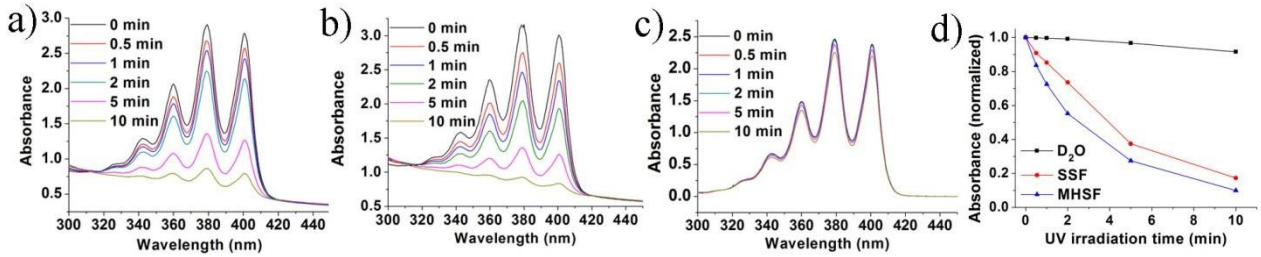

Fig.2 Photobleaching of ABDA by $^1O_2$ generated by (a) SSF nanoparticle suspension (0.5 mg/mL), (b) MHSF nanoparticle suspension (0.5 mg/mL), (c) pure D_2O and (d) Decay curves of OD at 376 nm as a function of UV irradiation time, corresponding to a-c.

To investigate the drug loading capacity and release behaviour of nanoparticles, doxorubicin (DOX), a potent first-line cytotoxic chemotherapeutic agent, was selected as the model anticancer drug in this study. It is found that MHSF possesses a loading capacity of 74 μg mg^{-1}, which is more than ten times higher than that of SSF (5 μg mg^{-1}). Such a significantly enhanced drug loading capacity is attributed to the much higher pore volume and surface area of MHSF than that of SSF (Table S1). Figure S5 shows the release profile of DOX from MHSF *in vitro* in acetate buffer (pH=5.5) and PBS (pH=7.4), which corresponds to the cancer cell endosome/lysosome and normal physical pH conditions, respectively. In both pH conditions, a relative fast release occurs within 1 h followed by a sustained release for more than 48. It is worth noting that the DOX release rate is much faster at pH 5.5 than at neutral pH. Approximately 50% of DOX is released within 24 h at pH 5.5, while less than 20% is released at pH 7.4. This faster release behaviour of DOX at a more acidic condition is ascribed to the higher hydrophilicity and solubility of DOX at lower pH due to increased protonation of NH_2 groups on DOX.[10c] Considering the practical application of MHSF for drug delivery, this pH dependant release behaviour is vitally important to minimize the cytotoxicity of drug to normal cells before reaching tumor sites.

The *in vitro* cytotoxicity of nanoparticles was tested in human breast adenocarcinoma cells (MCF-7) using MTT (3-(4,5-dimethylthiazol-2-yl)-2,5-diphenyltetrazolium bromide) assay. Figure S6 shows the cytotoxicity of SSF and MHSF at different concentrations (20, 40, 80 and 160 μg mL^{-1}). Both nanoparticles show negligible cytotoxic effect (<15%) on MCF-7 cells even at a high concentration up to 160 μg mL^{-1}, indicating their excellent biocompatibility.

The fluorescence and the cell uptake of MHSF were studied using confocal laser scanning microscopy (CLSM). The cell nuclei and cytoskeletons were stained with (4',6-diamidino-2-phenylindole (DAPI, blue) and Alexa Fluor® 488 phalloidin (green), respectively. As shown in Figure S7, no red fluorescence can be observed in cells without adding nanoparticles. After treating cell with 160 μg ml^{-1} of nanoparticle, red spots indicating MHSF were observed within green fluorescence, suggesting that the uptake of MHSF by MCF-7 cells is efficient and MHSF were

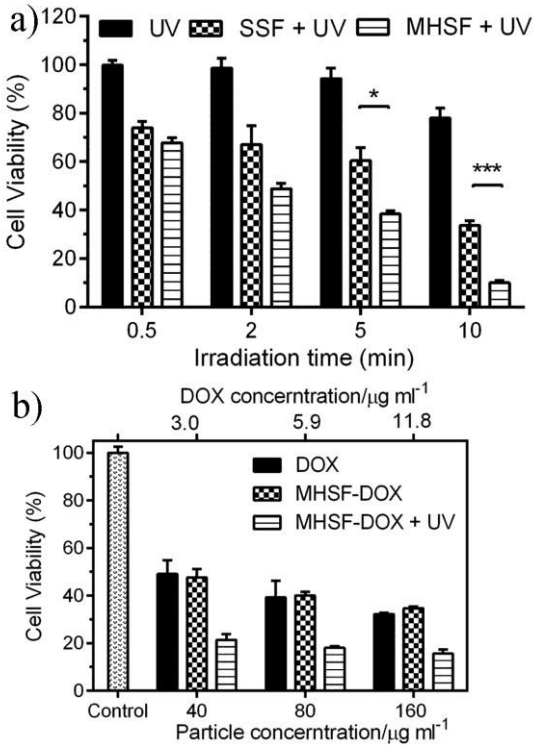

Fig.3 Cell viability of MCF-7 cells (a) treated with SSF or MHSF under different UV irradiation time at particle concentration of 160 μg/ml, (b) treated with DOX or MHSF-DOX in the absence or presence of UV irradiation for 5 min. * $p < 0.05$, *** $p < 0.001$ based on a t -test.

distributed in the cytoplasmic region. The red fluorescence generated from MHSF is attributed to the dispersed C_{60} molecules[16] in the silica framework with minimized self-quenching, offering an effective and convenient opportunity for intracellular nanoparticle tracking without functionalization of conventional organic dyes.

To investigate the therapeutic performance, the photodynamic activity of MHSF without loading DOX toward MCF-7 cells was firstly evaluated and compared with SSF. The cell viability as a function of UV irradiation time after treatment of SSF and MHSF is shown in Figure 3a. UV irradiation shows negligible cytotoxic

effect within 5 min, while a prolonged time to 10 min induces ~20% cell death. Therefore, we chose UV irradiation time of 5 min as the optimized time for the following chemo-/photodynamic therapeutic performance. The cell viability in the presence of SSF or MHSF exhibits an irradiation time dependent manner, decreasing from ~74% and ~68% at 0.5 min to 34% and 10% at 10 min, respectively. Interestingly, MHSF shows an enhanced cell inhibition compared to SSF at all irradiation times. Such enhancement becomes more significant at prolonged irradiation times. The superior photodynamic activity of MHSF can be explained by the enhanced $^1O_2$ generation, compared to SSF (Figure 2).

We then investigated the combined chemotherapy and PDT performance of DOX loaded MHSF. As shown in Figure 3b, free DOX and DOX loaded MHSF without UV treatment exhibits comparable cell inhibition in a dosage dependent manner (~52%, 60% and ~67% viability at 40, 80 and 160 μg/ml, respectively). After UV light treatment, the cell viability is further inhibited to ~21%，~18% and ~15% at nanoparticle concentrations of 40, 80 and 160 μg ml^{-1}, respectively, indicating a combined chemo-/photodynamic therapy, which offers remarkable therapeutic efficacy with lower requirement of drug dosage.

It is worth mentioning that compared to previous polymer-C_{60} based systems,[10a, 10b, 10d, 17] the PDT efficacy of MHSF is among the highest with cell viability down to ~10% (Figure 3c). Such an excellent PDT efficiency is presumably attributed to three reasons: 1) Our selective etching method is able to create both mesopores and micropores, which is important to facilitate the generation of $^1O_2$ through enhanced interaction between C_{60} and molecular oxygen; 2) The MHSF can be efficiently internalized into cells due to its excellent dispersity and suitable particle size (~ 50 nm);[18] 3) C_{60} are homogeneously dispersed in silica framework at molecular scale, which effectively minimize $^1O_2$ quenching.[13]

Conclusions

In summary, well dispersed mesoporous hollow silica-fullerene nanoparticles (MHSF) with particle size of ~50 nm have been prepared using a selective etching method. It is demonstrated that MHSF with higher porosity than that of solid silica-fullerene nanoparticle (SSF) shows significantly higher drug loading capacity and enhanced photodynamic activity. The drug loaded MHSF shows a faster release rate at pH 5.5 than pH 7.4, which is important for minimized pre-mature release. Moreover, the fluorescence generated due to the dispersed C_{60} in the silica matrix can be directly used for intracellular tracking. The combined chemo-/photodynamic therapy have been confirmed in cancer cells, leading to cell viability down to ~15%. The rationally designed porous silica-fullerene provides a multifunctional cancer therapy platform with intracellular traceability and excellent anticancer performance.

Acknowledgments

We acknowledge the support from the Australian Research Council, the Australian National Fabrication Facility and the Australian Microscopy and Microanalysis Research Facility at the Centre for Microscopy and Microanalysis, The University of Queensland.

Notes and references

[a]*Australian Institute for Bioengineering and Nanotechnology, The University of Queensland, Brisbane, QLD 4072, Australia. Fax: +61 7 3346 3973; Tel: +61 7 3346 3283; E-mail: c.yu@uq.edu.au;m.yu2@uq.edu.au*

†Electronic Supplementary Information (ESI) available: [details of any supplementary information available should be included here]. See DOI: 10.1039/b000000x/

1. S. H. Wu, C. Y. Mou and H. P. Lin, *Chem. Soc. Rev.*, **2013**, 42,3862-3875
2. Y. S. Li and J. L. Shi, *Adv. Mater.*, **2014**, 26,3176-3205
3. a) Y. Chen, C. Chu, Y. C. Zhou, Y. F. Ru, H. R. Chen, F. Chen, Q. J. He, Y. L. Zhang, L. L. Zhang and J. L. Shi, *Small*, **2011**, 7,2935-2944; b) L. Y. Xia, M. Q. Zhang, C. E. Yuan and M. Z. Rong, *J. Mater. Chem.*, **2011**, 21,9020-9026; c) W. R. Zhao, M. D. Lang, Y. S. Li, L. Li and J. L. Shi, *J. Mater. Chem.*, **2009**, 19,2778-2783
4. a) J. Zhang, S. Karmakar, M. H. Yu, N. Mitter, J. Zou and C. Z. Yu, *Small*, **2014**, 10,5068-5076; b) D. H. W. Hubert, M. Jung, P. M. Frederik, P. H. H. Bomans, J. Meuldijk and A. L. German, *Adv. Mater.*, **2000**, 12,1286-1290; c) Y. N. Yang, S. Karmakar, M. H. Yu, A. Popat and C. Z. Yu, *Chem. Lett.*, **2014**, 43,316-318
5. Y. Chen, H. R. Chen, L. M. Guo, Q. J. He, F. Chen, J. Zhou, J. W. Feng and J. L. Shi, *Acs Nano*, **2010**, 4,529-539
6. Y. J. Wong, L. F. Zhu, W. S. Teo, Y. W. Tan, Y. H. Yang, C. Wang and H. Y. Chen, *J. Am. Chem. Soc.*, **2011**, 133,11422-11425
7. Y. X. Hu, Q. Zhang, J. Goebl, T. R. Zhang and Y. D. Yin, *Phys. Chem. Chem. Phys.*, **2010**, 12,11836-11842
8. J. Lehar, A. S. Krueger, W. Avery, A. M. Heilbut, L. M. Johansen, E. R. Price, R. J. Rickles, G. F. Short, J. E. Staunton, X. W. Jin, M. S. Lee, G. R. Zimmermann and A. A. Borisy, *Nat. Biotechnol.*, **2009**, 27,659-666
9. A. Khdair, H. Handa, G. Z. Mao and J. Panyam, *Eur. J. Pharm. Biopharm.*, **2009**, 71,214-222
10. a) J. J. Shi, L. Wang, J. Gao, Y. Liu, J. Zhang, R. Ma, R. Y. Liu and Z. Z. Zhang, *Biomaterials*, **2014**, 35,5771-5784; b) J. Q. Fan, G. Fang, F. Zeng, X. D. Wang and S. Z. Wu, *Small*, **2013**, 9,613-621; c) T. T. Wang, L. Y. Zhang, Z. M. Su, C. G. Wang, Y. Liao and Q. Fu, *Acs Appl. Mater. Inter.*, **2011**, 3,2479-2486; d) J. J. Shi, X. Y. Yu, L. Wang, Y. Liu, J. Gao, J. Zhang, R. Ma, R. Y. Liu and Z. Z. Zhang, *Biomaterials*, **2013**, 34,9666-9677
11. S. Z. Wang, R. M. Gao, F. M. Zhou and M. Selke, *J. Mater. Chem.*, **2004**, 14,487-493
12. J. W. Arbogast, A. P. Darmanyan, C. S. Foote, Y. Rubin, F. N. Diederich, M. M. Alvarez, S. J. Anz and R. L. Whetten, *J. Phys. Chem.*, **1991**, 95,11-12
13. Z. Markovic and V. Trajkovic, *Biomaterials*, **2008**, 29,3561-3573
14. J. Jeong, M. Cho, Y. T. Lim, N. W. Song and B. H. Chung, *Angew. Chem. Int. Ed.*, **2009**, 48, 5296-5299
15. Y. S. Lin and C. L. Haynes, *Chem. Mater.*, **2009**, 21,3979-3986
16. J. Jeong, J. Jung, M. Choi, J. W. Kim, S. J. Chung, S. Lim, H. Lee and B. H. Chung, *Adv. Mater.*, **2012**, 24,1999-2003
17. a) W. Zhang, X. D. Gong, C. Liu, Y. Z. Piao, Y. Sun and G. W. Diao, *J. Mater. Chem. B*, **2014**, 2,5107-5115; b) K. Nobusawa, M. Akiyama, A. Ikeda and M. Naito, *J. Mater. Chem.*, **2012**, 22,22610-22613
18. F. Lu, S. H. Wu, Y. Hung and C. Y. Mou, *Small*, **2009**, 5,1408-1413